sciendo

DOI 10.2478/ama-2021-0006

acta mechanica et automatica, vol.15 no.1 (2021)

SELF-ADAPTIVE ASYMMETRICAL ARTIFICIAL POTENTIAL FIELD APPROACH DEDICATED TO THE PROBLEM OF POSITION TRACKING BY NONHOLONOMIC UAVS IN WINDY ENIVROMENTS

Cezary KOWNACKI*

*Department of Robotics and Mechatronics, Faculty of Mechanical Engineering, Bialystok University of Technology, ul. Wiejska 45C, 15-351 Białystok, Poland

c.kownacki@pb.edu.pl

received 26 May 2020, revised 27 April 2021, accepted 30 April 2021

Abstract: Artificial potential fields (APFs) are a popular method of planning and controlling the path of robot movement, including unmanned aerial vehicles (UAVs). However, in the case of nonholonomic robots such as fixed-wing UAVs, the distribution of velocity vectors should be adapted to their limited manoeuvrability to ensure stable and precise position tracking. The previously proposed local asymmetrical potential field resolves this issue, but it is not effective in the case of windy environments, where the UAV is unable to maintain the desired position and drifts due to the wind drift effect. This is reflected in the growth of position error, which, similar to the steady-state error in the best case, is constant. To compensate for it, the asymmetrical potential field approach is modified by extending definitions of potential function gradient and velocity vector field (VVF) with elements based on the integral of position tracking error. In the case of wind drift, the value of this integral increases over time, and lengths and orientations of velocity vectors will also be changed. The work proves that redefining gradient and velocity vector as a function of position tracking error integrals allows for minimisation of the position tracking error caused by wind drift.

Key words: artificial potential field, asymmetrical potential field, position tracking, UAV, self-adaptive potential field

1. INTRODUCTION

The field of unmanned aerial vehicles (UAVs) is one of the most rapidly developing ones in the field of robotics. Intensive research on technology and algorithms applied in UAVs is making them more and more autonomous. However, there remains much work to be done on core topics such as obstacle avoidance, path planning or formation flight to make them fully autonomous. The major contribution of UAVs to military or civil applications belongs to unmanned multirotor vehicles, their main advantage being their capability of hovering. This makes it easier to control a flight path, especially in an urban environment with plenty of obstacles. Unfortunately, the endurance of multi-rotor flights is limited as a result of their low power efficiency. Missions of fixed-wing UAVs are longer, but due to their limited manoeuverability as nonholonomic vehicles, it is more difficult to precisely control the flight path. This particularly concerns such applications as obstacle avoidance, path planning or formation flight under windy conditions.

Artificial potential field (APF) methods are a convenient way to implement precise and stable position control in applications of position guidance or obstacle avoidance, and this also applies in the case of UAVs (Frew et al., 2007). The main advantage of APF comes from the fact that potential functions are Lyapunov functions with local minimums. This ensures asymptotically stable control of robot position to achieve the desired shape of the path. Therefore, various approaches to APF are widely applied in algorithms dedicated to problems of obstacle avoidance discussed in Budiyanto et al. (2015) and Nieuwenhuisen et al. (2013), path planning methods with movement among obstacles described in Chen et al. (2016), Hatton and Choset (2011), Khuswendi et al. (2011), Mukherjee and Anderson (1993) and Nelson et al. (2007), formation flights presented in Barnes et al. (2007), Bennet and McInnes (2011), Bennet and McInnes (2008), Kokume and Uchiyama (2010), Kownacki and Ambroziak (2017), Nagao and Uchiyama (2014), Tobias et al. (2008), Suzuki and Uchiyama (2011) and Suzuki and Uchiyama (2010) or their combinations given in Cetin and Yilmaz (2016), Chen et al. (2015) and Mukherjee and Anderson (1993). Even the rules of birds flocking, i.e. repulsion and cohesion, which are applied in formation flights, can be considered implementations of APF (Kownacki and Ołdziej, 2016; Virágh et al., 2014). APF precisely and clearly defines a relation between the velocity vector designating a specific guidance route and the actual position relative to other UAVs, obstacles or mission targets (Frew et al., 2007). As mentioned in Nagao and Uchiyama (2014), known APFs applied in the majority of articles concerning APF, also in those referred above, fail in the case of position tracking by nonholonomic vehicles. Typically, APF's definitions provide a symmetrical distribution of velocity vectors around their minimums. This, combined with nonholonomic constraints, leads to instability that manifests as violent changes of airspeed and heading angle (Frew et al., 2007; Kownacki and Ambroziak, 2017). This happens when a UAV is just near the point of tracked position and position tracking error decreases towards zero. Then, even small unintentional displacement produces a violent change of the desired heading. Violent changes of heading can be explained by the fact that it is usually calculated from the ratio of position differences on the x and y axes of a navigational coordinate frame and the arctangent

function. The varying ratio of distances on the x and y axes, from low values to high, occurring when both distance values oscillate around zero, results in significantly different values of angle according to the curve of arctangent.

The circular potential function based on a sigmoid function is one of the ideas meant to prevent these violent changes of heading values and achieve a circular loiter pattern tracked by the UAV. Its effectiveness is the result of the symmetrical gradient distribution on both sides of the circular flight pattern, attracting the UAV to its line (Frew et al., 2007; Nagao and Uchiyama, 2014). The flight pattern is a local minimum of the attractive potential function created as a combination of circular sigmoid functions. In turn, in work of Kownacki and Ambroziak (2017), the novel approach based on an asymmetrical artificial potential function (AAPF), defined in a local coordinate system, provides position tracking stability in the case of formation flights of nonholonomic fixed-wing UAVs. The definition of the asymmetrical potential function is used to create a velocity vector field (VVF), which guides a fixed-wing UAV in a way that smoothly aligns its heading and airspeed to the heading angle and airspeed of the tracked point. In the subsequent work (Kownacki and Ambroziak, 2019), the approach is modified by expanding it by a rotation mechanism of the VVF. It counteracts increments of tracking error during manoeuvres as the result of formation rotation when a UAV is behind the leader and the tracked position.

Unfortunately, none of the examples of application of artificial potential functions that are available in the literature account for external disturbances such as wind drift. A VVF is a geometrical representation of the relation between the expected direction of a UAV's movement and its positions relative to a reference point. In turn, wind treated as the movement of air mass with a constant velocity can be represented by a homogeneous VVF. Thus, combining the guidance VVF with the wind velocity vector field (WVVF) causes a UAV to drift from the desired position and its desired path of flight. The issue is especially important for nonholonomic UAVs. Therefore, this work proposes a self-adaptive asymmetrical potential function mechanism which prevents such drift error, having the meaning of the steady-state error. The effectiveness of the presented adaptation mechanism is proven by the numerical simulation results discussed in Section 5. The idea of the mechanism is to consider integrals of tracking errors in definitions of potential function gradient and VVF only if there is any constant movement of air mass causing wind drift. The slope of the potential function, spatial orientation and lengths of gradients and velocity vectors will be changing depending on wind drift incrementing the integrals' values. Therefore, the main contribution of this work is defining a new approach to the asymmetrical potential function from works of Kownacki and Ambroziak (2017) and Kownacki and Ambroziak (2019), which considers integrals of position tracking errors so as to minimise them in the case of wind drift effect.

The next part of the article is divided into four sections. The first one formulates the problem of wind drift increasing position tracking error and producing a steady-state error. The second section presents new definitions of potential function gradient and VVF, which are based on the asymmetrical potential function approach modified by a self-adaptive mechanism applying integrals of tracking error. In the third section, the results of numerical simulations compare responses to a step change of wind velocity in the cases of the proposed novel self-adaptive asymmetrical potential function approach and the previous approach from Kownacki and Ambroziak (2019). The conclusions and discussion are in the final section.

2. PROBLEM FORMULATION

Flight control based on artificial potential functions is convenient as it transforms geometrical relations between a UAV's position and characteristic mission points into a VVF which accomplishes predefined rules of guidance, e.g. obstacle avoidance. Velocity vectors implementing guidance rules are used to calculate navigational parameters such as desired heading and pitch angles and desired airspeed. These parameters are mostly controlled by traditional PID (Proportional–Integral–Derivative) control loops with a two-level structure (Kownacki and Ambroziak, 2017; Kownacki and Ambroziak, 2019). Unfortunately, reaching the desired values of heading and pitch angles and airspeed by a UAV does not guarantee that flight will be controlled stably in the steady state. In windy environments, where there is a constant wind treated as the flow of air mass, the flight guidance of nonholonomic UAVs can be disturbed, especially if it is a crosswind. What results is that the ground speed of fixed-wing UAVs is the sum of True Air Speed (TAS) and wind speed, and in aviation, this is called the wind drift effect. The problem of wind drift is presented in Fig. 1a, where the asymmetrical artificial potential field (AAPF) approach is applied to track a moving point associated with the origin of a local coordinate system $Ox_{Pi}y_{Pi}z_{Pi}$. Arrows labelled with symbols V_T, V_W, V_G, and V_{UAV} represent, respectively, the velocity vector of the frame $Ox_{Pi}y_{Pi}z_{Pi}$ (the velocity of the tracked point), the velocity vector of wind, the airspeed vector of the UAV obtained from the AAPF and the ground speed vector, which is the sum of the last two. Thus, the final flight path will be determined by the velocity vector V_{UAV}, not by the velocity vector field V_G.

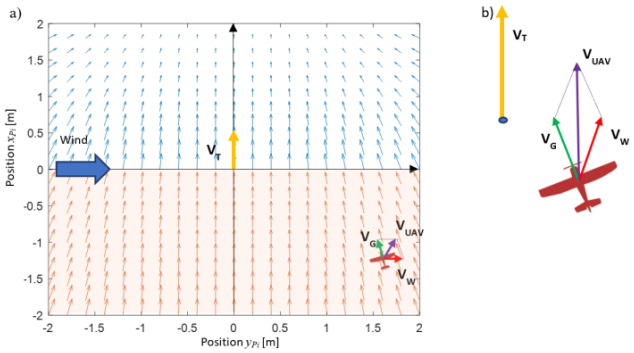

Fig. 1. A flight scenario when wind drift disturbs flight guidance based on the artificial asymmetrical potential field: (a) control of position tracking based on AAPF in the case of constant wind presence. There is an angle between the reference velocity vector V_G given by AAPF and the ground speed vector V_{UAV}, which is called the drift angle. (b) the UAV is unable to reach a tracked position due to its resultant ground speed vector V_{UAV} being parallel to the velocity vector of the tracked position. AAPF - asymmetrical artificial potential field, UAV - unmanned aerial vehicle

In Fig. 1b, there is a case where the UAV is unable to reach its desired position due to the fact that ground speed vector V_{UAV} is parallel to the velocity vector of the tracked position V_T. Therefore, the relative positions, i.e. the position tracking error, will be

DOI 10.2478/ama-2021-0006

constant in the steady-state. For this and similar cases, constant wind can be considered as a homogenous VVF that modifies the tracking guidance, accordingly to the superposition of both fields of the velocity vector (Fig. 2). The superposition of these two fields makes it impossible for a fixed-wing UAV to achieve precise position tracking. Therefore, the VVF constructed on AAPF should not be constant over time, but should change automatically in a way that minimises any position error in the steady-state caused by wind drift. The most convenient and simplest way to minimise errors in the steady state is to include integrals of these errors in the definitions of the VVF. The novel definition of the VVF based on the AAPF approach for fixed-wing UAVs is given in the next section. The method, which utilises this novel definition, is called the self-adaptive AAPF approach, and it is addressed to the problem of wind drift for nonholonomic UAVs.

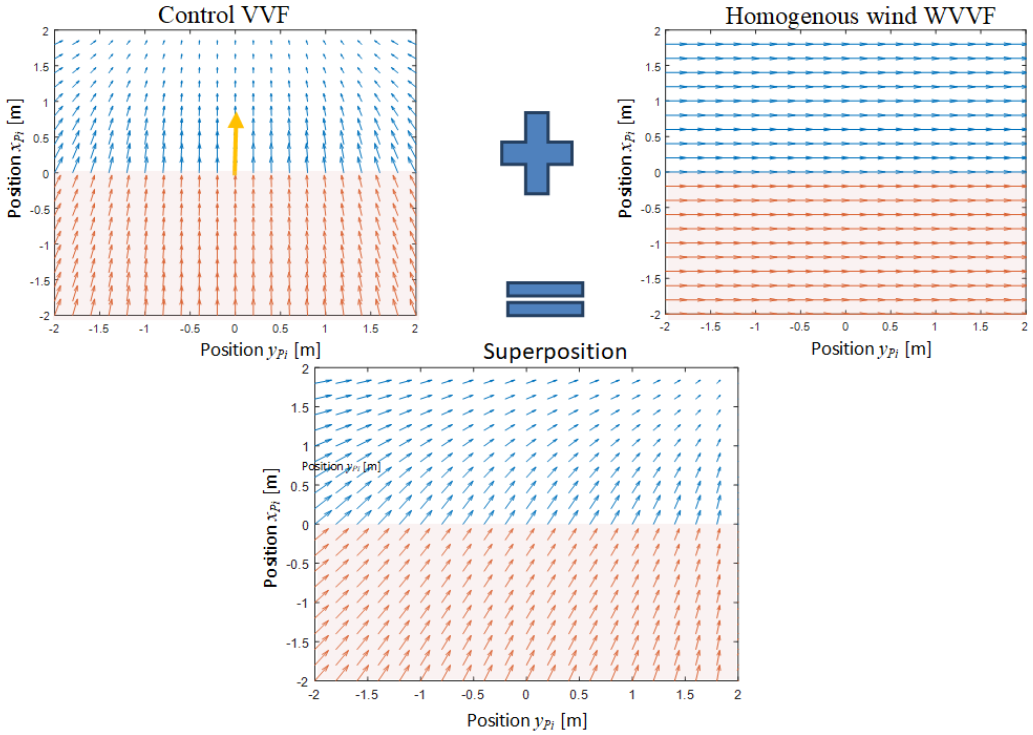

Fig. 2. A superposition of the VVF given by AAPF and the WVVF, modifying guidance and disabling the possibility of precise position tracking. AAPF - asymmetrical artificial potential field; VVF - velocity vector field; WVVF - wind velocity vector field.

3. SELF-ADAPTIVE ASYMMETRICAL POTENTIAL FIELD

The AAPF ensures stable position tracking in the case of nonholonomic UAVs, which is proven in Kownacki and Ambroziak (2017). In turn, the rotation mechanism described in Kownacki and Ambroziak (2019) minimises tracking error during manoeuvres when nonholonomic UAVs fly in a rigid formation. The novel approach proposed in this work is also dedicated to nonholonomic vehicles; hence, the definition of AAPF from Kownacki and Ambroziak (2017) and Kownacki and Ambroziak (2019) will be the starting point. Let us consider a scenario where a UAV tracks a virtual point which is simultaneously the origin of a local coordinate system $Ox_{Pi}y_{Pi}z_{Pi}$. Spatial orientations of axes x_{Pi}, y_{Pi} and z_{Pi} are determined by vertical and horizontal movements of that point in the global coordinate system $Ox_Gy_Gz_G$. UAV coordinates given in the frame $Ox_{Pi}y_{Pi}z_{Pi}$ are values of tracking errors. The proposed novel approach aims to minimise values of those coordinates when a fixed-wing UAV flies under windy conditions.

The definition of AAPF U_i^S will be the same as in Kownacki and Ambroziak (2017) and Kownacki and Ambroziak (2019):

$$U_i^S(x_{Pi}, y_{Pi}, z_{Pi}) = \begin{cases} V_L \cdot \arctan(\alpha \cdot x_{Pi}) + \frac{1}{3} \cdot \gamma \cdot |{y_{Pi}}^3| + \frac{1}{3} \cdot \gamma \cdot |{z_{Pi}}^3|, x_{Pi} \geq 0 \\ V_L \cdot |\alpha \cdot x_{Pi}| + \frac{1}{3} \cdot \beta \cdot |{x_{Pi}}^3| + \frac{1}{3} \cdot \gamma \cdot |{y_{Pi}}^3| + \frac{1}{3} \cdot \gamma \cdot |{z_{Pi}}^3|, x_{Pi} < 0 \end{cases} \quad (1)$$

where V_L – is the airspeed of the tracked virtual point, α, β, γ – coefficients regulating the slope of the potential function, i.e. in the forward longitudinal direction; ($x_{Pi}>0$) – rate of deceleration, in backward direction; ($x_{Pi}<0$) – rate of acceleration, and in both perpendicular directions, lateral and vertical; (y_{Pi} and z_{Pi}) – respectively, rate of heading and pitch.

According to Kownacki and Ambroziak (2017) and Kownacki and Ambroziak (2019), the gradient of the potential function U_i^S is as follows:

$$\nabla U_i^S(x_{Pi}, y_{Pi}, z_{Pi}) = \begin{cases} \left[\frac{\alpha \cdot V_L}{1+(\alpha \cdot x_{Pi})^2}, \gamma \cdot sgn(y_{Pi}) \cdot {y_{Pi}}^2, \gamma \cdot sgn(z_{Pi}) \cdot {z_{Pi}}^2\right], x_{Pi} \geq 0 \\ \left[sgn(x_{Pi}) \cdot (\alpha \cdot V_L + \beta \cdot {x_{Pi}}^2), \gamma \cdot sgn(y_{Pi}) \cdot {y_{Pi}}^2, \gamma \cdot sgn(z_{Pi}) \cdot {z_{Pi}}^2\right], x_{Pi} < 0 \end{cases} \quad (2)$$

The gradient ∇U_i^S is only a function of the relative position given in the local frame $Ox_{Pi}y_{Pi}z_{Pi}$. As shown in Fig. 1b, it can be insensitive to position tracking error at the steady state as a result of wind drift. Therefore, gradient definition (2) must be modified in a way that relates gradient components to cumulative tracking error expressed by its integral. According to Kownacki and Ambroziak (2017) and Kownacki and Ambroziak (2019), gradient ∇U_i^S is the basis for creating the VVF that is used to calculate the desired heading, pitch and airspeed. Therefore, if the integral of tracking error modifies elements of gradient ∇U_i^S, it will affect UAV guidance.

Modifications of gradient definition (2) on the longitudinal axis x_{Pi} will first be discussed. To minimise the steady-state tracking error on axis x_{Pi}, the length of gradient ∇U_i^S and the length of the related velocity vector V_i^S on this axis should be changed according to the increasing integral of tracking error. For $x_{Pi} \geq 0$, the lengths should be decreased, and for $x_{Pi} < 0$, increased.

Therefore, the definition of the potential function gradient (2) must be modified by inserting coefficients dependent on the current value of the integral I_X. It adapts the gradient length on axis x_{Pi} with a strength depending on the values of gains δ_{x1}, δ_{x2}. The modified gradient ∇U_i^{AD} is defined by Eq. (3), and differences between definitions (2) and (3) are highlighted by bold font. In Eq. (2), coefficients on x_{Pi}, i.e. α and β, are constant over time. In Eq. (3), these coefficients are, respectively, the sum of α and $\delta_{x1} \cdot |I_X|$ and the sum of β and $\delta_{x2} \cdot |I_X|$; therefore, they are time-variant and depend on the constant tracking error caused by wind drift.

To formulate a new definition of velocity vector field V_i^S, gradient ∇U_i^S must be replaced with ∇U_i^{AD}. However, for the y_{Pi} and z_{Pi} axes, both definitions (2) and (3) are identical. To change values of desired heading and pitch angles, it is necessary to introduce compensation vector I, which is a function of integrals I_Y and I_Z.

$$\nabla U_i^{AD}(x_{Pi}, y_{Pi}, z_{Pi}) = \begin{cases} \left[\frac{\alpha \cdot V_L}{1+(\alpha+\boldsymbol{\delta_{x1}} \cdot |\boldsymbol{I_X}|)^2 \cdot x_{Pi}^2}, \gamma \cdot sgn(y_{Pi}) \cdot {y_{Pi}}^2, \gamma \cdot sgn(z_{Pi}) \cdot {z_{Pi}}^2\right], x_{Pi} \geq 0 \\ \left[sgn(x_{Pi}) \cdot (\alpha \cdot V_L + (\beta + \boldsymbol{\delta_{x2}} \cdot |\boldsymbol{I_X}|) \cdot {x_{Pi}}^2), \gamma \cdot sgn(y_{Pi}) \cdot {y_{Pi}}^2, \gamma \cdot sgn(z_{Pi}) \cdot {z_{Pi}}^2\right], x_{Pi} < 0 \end{cases} \quad (3)$$

where I_X – is the value of the integral (Eq. 3) on axis x_{Pi}, δ_{x1}, δ_{x2} – gains of I_X.

$$I_X = \begin{cases} \int_0^t x_{Pi} d\tau \ , (x_{Pi} \geq 0 \ \cap \int_0^t x_{Pi} d\tau \geq 0) \ \cup (x_{Pi} < 0 \ \cap \int_0^t x_{Pi} d\tau \leq 0) \\ 0 \end{cases} \quad (4)$$

$$V_i^S(x_{Pi}, y_{Pi}, z_{Pi}) = \begin{bmatrix} \nabla U_i^S(x_{Pi}) \\ -\nabla U_i^S(y_{Pi}) \\ -\nabla U_i^S(z_{Pi}) \end{bmatrix} \cdot D(\dot{\Psi}_L) \quad (5)$$

These integrals have the same role as integral I_X in Eq. (3), but they are used to compensate wind drift on axes y_{Pi} and z_{Pi} by changing the direction of flight defined by heading and pitch angles. The value of integral I_X has an impact on the x_{Pi}-axis component of gradient ∇U_i^{AD} only when the sign of integral $\int_0^t x_{Pi} d\tau$ is the same as the sign of x_{Pi}. Otherwise, the value of I_X equals zero, and the definition of the gradient ∇U_i^{AD} is identical to that of ∇U_i^S. This rule is necessary, because integral I_X should compensate for wind drift as follows: its negative value should only accelerate the UAV when $x_{Pi} < 0$ and its positive value should decelerate the UAV only when $x_{Pi} \geq 0$ (Fig. 3). For other cases, gradient ∇U_i^{AD} must be the same as gradient ∇U_i^S to prevent oscillations. Therefore, the sign of integral I_X must be correlated with the sign of x_{Pi}, and its change switches guidance rules on axis x_{Pi} between ∇U_i^{AD} and ∇U_i^S (Fig. 3). This happens when the UAV crosses the *y*-*z* plane.

The next modifications related to the novelty of the self-adaptive asymmetrical potential function are addressed directly to velocity vector field V_i^S from Kownacki and Ambroziak (2019). Velocity vector field V_i^S based on gradient ∇U_i^S is given by Eq. (5) (Kownacki and Ambroziak, 2019).

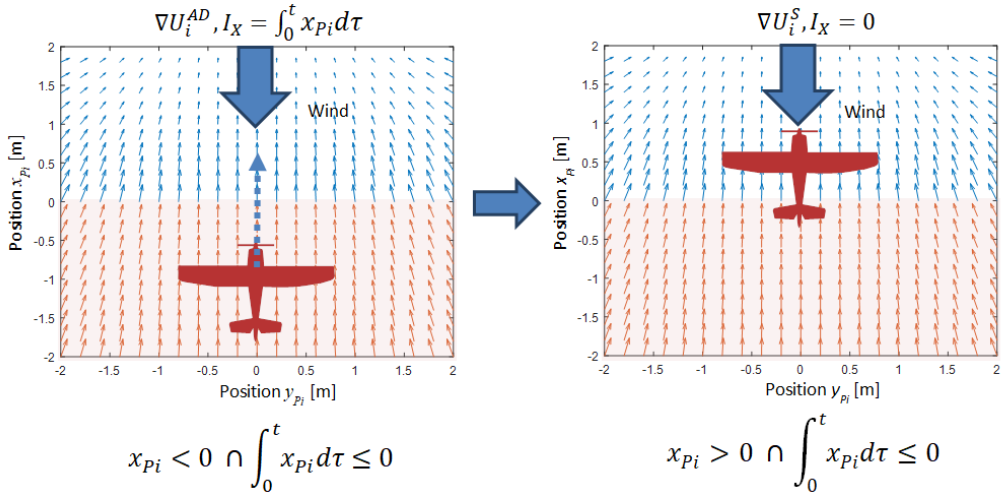

Fig. 3. Switching between gradient ∇U_i^{AD} and ∇U_i^S when the UAV flies behind the tracked position and then crosses the y-z plane. UAV, unmanned aerial vehicles

The definition of velocity vector field V_i^{AD} applied in the self-adaptive approach is as follows:

$$V_i^{AD}(x_{Pi}, y_{Pi}, z_{Pi}) = \left[\begin{bmatrix} \nabla U_i^{AD}(x_{Pi}) \\ -\nabla U_i^{AD}(y_{Pi}) \\ -\nabla U_i^{AD}(z_{Pi}) \end{bmatrix} + I\right] \cdot D(\dot{\Psi}_L) =$$
$$\left(\begin{bmatrix} \left|\nabla U_i^{AD}(x_{Pi})\right| \\ -\nabla U_i^{AD}(y_{Pi}) \\ -\nabla U_i^{AD}(z_{Pi}) \end{bmatrix} - \begin{bmatrix} 0 \\ \delta_y \cdot |I_Y| \cdot sgn(y_{Pi}) \cdot {y_{Pi}}^2 \\ \delta_z \cdot |I_Z| \cdot sgn(z_{Pi}) \cdot {z_{Pi}}^2 \end{bmatrix}\right) \cdot \begin{bmatrix} \cos(\varepsilon \cdot \dot{\Psi}_L) & \sin(\varepsilon \cdot \dot{\Psi}_L) & 0 \\ -\sin(\varepsilon \cdot \dot{\Psi}_L) & \cos(\varepsilon \cdot \dot{\Psi}_L) & 0 \\ 0 & 0 & 1 \end{bmatrix} \quad (6)$$

where $\dot{\Psi}_L$ – is the rate of heading angle of the tracked virtual point; ε – gain coefficient having the meaning of the time constant related to inertia of response to tracked point turns; I – compensation vector dependent on integrals of tracking errors on the y-axis (I_Y) and z-axis (I_Z); and δ_y, δ_z – gains of integrals I_Y and I_Z, respectively.

Definitions of the integral values I_Y and I_Z are given below:

$$I_Y = \begin{cases} \int_0^t y_{Pi} d\tau \ , (y_{Pi} \geq 0 \ \cap \int_0^t y_{Pi} d\tau \geq 0) \ \cup (y_{Pi} < 0 \ \cap \int_0^t y_{Pi} d\tau \leq 0) \\ 0 \end{cases} \quad (7)$$

$$I_Z = \begin{cases} \int_0^t z_{Pi} d\tau \ , (z_{Pi} \geq 0 \ \cap \int_0^t z_{Pi} d\tau \geq 0) \ \cup (z_{Pi} < 0 \ \cap \int_0^t z_{Pi} d\tau \leq 0) \\ 0 \end{cases} \quad (8)$$

where z_{Pi}, y_{Pi} – are UAV coordinates (tracking errors) on axes z_{Pi} and y_{Pi} of frame $Ox_{Pi}y_{Pi}z_{Pi}$.

Integrals I_Y and I_Z modify lengths of velocity vectors V_i^{AD} on the z_{Pi} and y_{Pi} axes, which changes both lengths and spatial orientations of velocity vectors. Also, in this case, the signs of integrals I_Y and I_Z must be the same as the signs of tracking errors on the y_{Pi} and z_{Pi} axes. Otherwise, values of these integrals should equal zero, and Eq. (6) becomes the same as Eq. (5), or almost the same when ∇U_i^{AD} is identical to ∇U_i^S for I_X different from zero. This switching prevents situations when the UAV crosses planes defined by axes x_{Pi}-z_{Pi} or x_{Pi}-y_{Pi}, and the sign of the corresponding tracking error on the y_{Pi} or z_{Pi} axis is reversed. If the integrals I_Y or I_Z are non-zero values with signs opposite to tracking errors, velocity vector field V_i^{AD} will guide the UAV in the same direction as the wind, and the wind drift effect will be amplified. This could cause position oscillations on the y_{Pi} or z_{Pi} axis. Therefore, the compensation should work only in the direction opposite to the wind (Fig. 4).

In the next section, results of numerical simulations prove that the novel self-adaptive potential field approach, which uses integrals I_X, I_Y and I_Z to modify gradient ∇U_i^{AD} and velocity vector field V_i^{AD}, effectively minimises the steady-state tracking error caused by the wind.

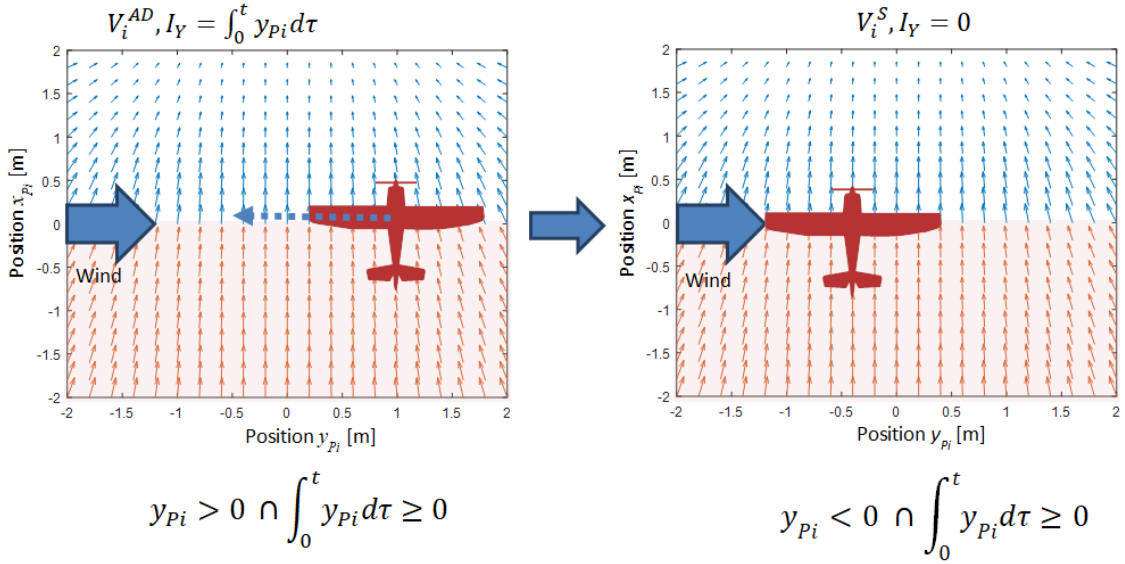

Fig. 4. Switching between V_i^{AD} and V_i^S when the UAV flies to the left of the tracked position and then crosses the x-z plane. UAV - unmanned aerial vehicles

4. NUMERICAL SIMULATIONS

In numerical simulations, the same dynamical model of a fixed-wing UAV was utilised as in works of Kownacki and Ambroziak (2017) and Kownacki and Ambroziak (2019). The UAV's dynamics are defined by a set of six differential equations, namely Eqs (9) and (10):

$$\begin{bmatrix} \dot{u} \\ \dot{v} \\ \dot{w} \end{bmatrix} = \begin{bmatrix} r \cdot v - q \cdot w \\ p \cdot w - r \cdot u \\ q \cdot u - p \cdot v \end{bmatrix} + \frac{1}{m} \cdot \begin{bmatrix} F_x \\ F_y \\ F_z \end{bmatrix} \quad (9)$$

$$\begin{bmatrix}\dot{p}\\ \dot{q}\\ \dot{r}\end{bmatrix}=\begin{bmatrix}\frac{I_{xz}\cdot(I_x-I_y+I_z)}{I_x\cdot I_z-I_{xz}^2}\cdot p\cdot q-\frac{I_z(I_z-I_y)+I_{xz}^2}{I_x\cdot I_z-I_{xz}^2}\cdot q\cdot r+\frac{I_z}{I_x\cdot I_z-I_{xz}^2}\cdot L+\frac{I_{xy}}{I_x\cdot I_z-I_{xz}^2}\cdot N\\ \frac{I_z-I_x}{I_y}\cdot p\cdot r-\frac{I_{xz}}{I_y}(p^2-r^2)+\frac{1}{I_y}\cdot M\\ \frac{I_x(I_x-I_y)+I_{xz}^2}{I_x\cdot I_z-I_{xz}^2}\cdot p\cdot q-\frac{I_{xz}\cdot(I_x-I_y+I_z)}{I_x\cdot I_z-I_{xz}^2}\cdot q\cdot r+\frac{I_{xz}}{I_x\cdot I_z-I_{xz}^2}\cdot L+\frac{I_x}{I_x\cdot I_z-I_{xz}^2}\cdot N\end{bmatrix} \quad (10)$$

where F_x, F_y, F_z – are components of the total force vector applied to the UAV i.e. the sum of aerodynamic forces, force of gravity, and the force of the propulsion system; *L, M, N* – moments on the *x*, *y* and *z* axis, respectively; I_x, I_y, I_z – mass moments of inertia around the *x, y, z* axes, respectively, of the UAV body frame; I_{xz} – product of inertia for the *x* – *z* symmetry plane; *p, q, r* – angular velocities of banking, tilt, deflection; *u, v, w* – linear velocities; and *m* – mass of the vehicle.

Equations of the related kinematic model describing both position and orientation in the global frame *G* are given by Ambroziak and Gosiewski (2015) and Kownacki and Ambroziak (2017):

$$\begin{bmatrix}\dot{x}_G\\ \dot{y}_G\\ \dot{z}_G\end{bmatrix}=\begin{bmatrix}\cos(\Theta)\cdot\cos(\Psi) & \sin(\phi)\cdot\sin(\Theta)\cdot\cos(\Psi)-\cos(\phi)\cdot\sin(\Psi) & \cos(\phi)\cdot\sin(\Theta)\cdot\cos(\Psi)+\sin(\phi)\cdot\sin(\Psi)\\ \cos(\Theta)\cdot\sin(\Psi) & \sin(\phi)\cdot\sin(\Theta)\cdot\sin(\Psi)+\cos(\phi)\cdot\cos(\Psi) & \cos(\phi)\cdot\sin(\Theta)\cdot\sin(\Psi)-\sin(\phi)\cdot\sin(\Psi)\\ -\sin(\Theta) & \sin(\phi)\cdot\cos(\Theta) & \cos(\phi)\cdot\cos(\Theta)\end{bmatrix}\cdot\begin{bmatrix}u\\ v\\ w\end{bmatrix} \quad (11)$$

$$\begin{bmatrix}\dot{\phi}\\ \dot{\Theta}\\ \dot{\Psi}\end{bmatrix}=\begin{bmatrix}1 & \sin(\phi)\cdot tan(\Theta) & \cos(\phi)\cdot tan(\Theta)\\ 0 & \cos(\phi) & -\sin(\phi)\\ 0 & \frac{\sin(\phi)}{\cos(\Theta)} & \frac{\cos(\phi)}{\cos(\Theta)}\end{bmatrix}\cdot\begin{bmatrix}p\\ q\\ r\end{bmatrix} \quad (12)$$

where ϕ, Θ, Ψ – are the orientation angles of roll, pitch and heading angle, respectively; *p, q, r* – angular velocities of banking, tilt, deflection; *u, v, w* – linear velocities; and x_G, y_G, z_G – coordinates in the G frame.

The sum of forces applied to the body frame of a fixed-wing UAV is as follows (Ambroziak and Gosiewski, 2015; Kownacki and Ambroziak, 2017):

$$F=\begin{bmatrix}F_x\\ F_y\\ F_z\end{bmatrix}=\begin{bmatrix}-mg\cdot\sin(\Theta)\\ mg\cdot\cos(\Theta)\cdot\sin(\phi)\\ mg\cdot\cos(\Theta)\cdot\cos(\phi)\end{bmatrix}+\begin{bmatrix}F_p\\ 0\\ 0\end{bmatrix}+\begin{bmatrix}F_x^a\\ F_y^a\\ F_z^a\end{bmatrix} \quad (13)$$

where: *mg* – force of gravity, F_p – propulsion force (Eq. 12), F_z^a – lifting force, F_x^a – drag force, F_y^a – lateral force.

The force F_p generated by the propulsion system, i.e. propeller and electrical engine, is modelled by the equation (Ambroziak and Gosiewski, 2015; Kownacki and Ambroziak, 2017):

$$F_p=\frac{A\cdot\rho\cdot[(k_m\cdot\delta_t)^2-V_A^2]}{2} \quad (14)$$

where V_A – is airspeed of UAV; ρ – air density; k_m – the relation between throttle control signal, δ_t and engine revolutions; and *A* – the area swept out by the propeller blade.

The sum of aerodynamic moments and the moment generated by the propulsion system are given as follows (Ambroziak and Gosiewski, 2015; Kownacki and Ambroziak, 2017):

$$\begin{bmatrix}L\\ M\\ N\end{bmatrix}=\begin{bmatrix}0\\ M_p\\ 0\end{bmatrix}+\begin{bmatrix}L_a\\ M_a\\ N_a\end{bmatrix}=\begin{bmatrix}0\\ -k_t\cdot(k_m\cdot\delta_t)^2\\ 0\end{bmatrix}+\begin{bmatrix}L_a\\ M_a\\ N_a\end{bmatrix} \quad (15)$$

where M_p – is the moment generated by the propulsion system if the axis of propeller rotation coincides with the *x*-axis of the UAV's body; L_a – rolling moment; M_a – pitching moment; N_a – yawing moment; k_m – relation between throttle control signal, δ_t and engine revolutions; and k_t – coefficient of propeller torque.

Aerodynamic moments L_a, M_a, N_a are functions of control surface deflections, respectively: δ_a – ailerons (roll angle), δ_e - elevator (pitch angle) and δ_r – rudder (yaw angle). In turn, the propulsion force F_p is a function of throttle δ_t. Deflections δ_a, δ_e and throttle δ_t are outputs of lateral and longitudinal controls of the UAV, which are based on PID loops as shown in Fig. 5.

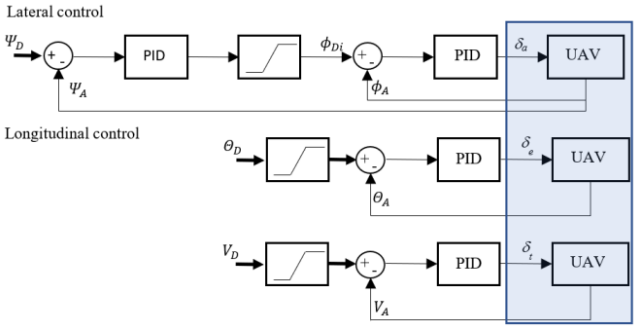

Fig. 5. Lateral and longitudinal control of the i-th UAV based on PID loops. Ψ_{Di} and Ψ_{Ai} – respectively, desired and actual heading; Φ_{Di} and Φ_{Ai} – respectively, desired and actual roll angle; Θ_{Di} and Θ_{Ai} – respectively, desired and actual pitch angle; V_{Di} and V_{Ai} – respectively, desired and actual airspeed (Kownacki and Ambroziak, 2017). UAV - unmanned aerial vehicle

Desired values of heading angle Ψ_{Di}, pitch angle Θ_{Di} and airspeed V_{Di} can be simply obtained from velocity vector field V_i^{AD} as given by equations (Kownacki C. and Ambroziak L., 2019; Kownacki C. and Ambroziak L., 2019):

$$\Psi_{Di}=atan2\left(V_i^{AD}(y_{Pi}),V_i^{AD}(x_{Pi})\right) \quad (16)$$

$$\Theta_{Di}=atan2\left(V_i^{AD}(z_{Pi}),\sqrt{V_i^{AD}(x_{Pi})^2+V_i^{SD}(y_{Pi})^2}\right) \quad (17)$$

$$V_{Di}=\sqrt{V_i^{AD}(x_{Pi})^2+V_i^{AD}(y_{Pi})^2+V_i^{AD}(z_{Pi})^2} \quad (18)$$

To verify the effectiveness of the proposed changes in the novel definitions of gradient V_i^{AD} and related velocity vector field V_i^{AD}, numerical simulations considering two scenarios were prepared. In each of them, the fixed-wing UAV follows a virtual point which is its desired position. Therefore, if the position tracking

algorithm is effective in minimising tracking errors, both flight paths, i.e. the flight path of the UAV and the reference trajectory of the virtual point, should overlap. During simulated flights, a step change of wind velocity is generated to observe the response of lateral and longitudinal controls based on the proposed self-adaptive approach. In each scenario, the direction of the wind is different, which makes separate verification of lateral and longitudinal guidance possible (Fig. 6). In the next section, flight paths and time plots of tracking errors present the results achieved.

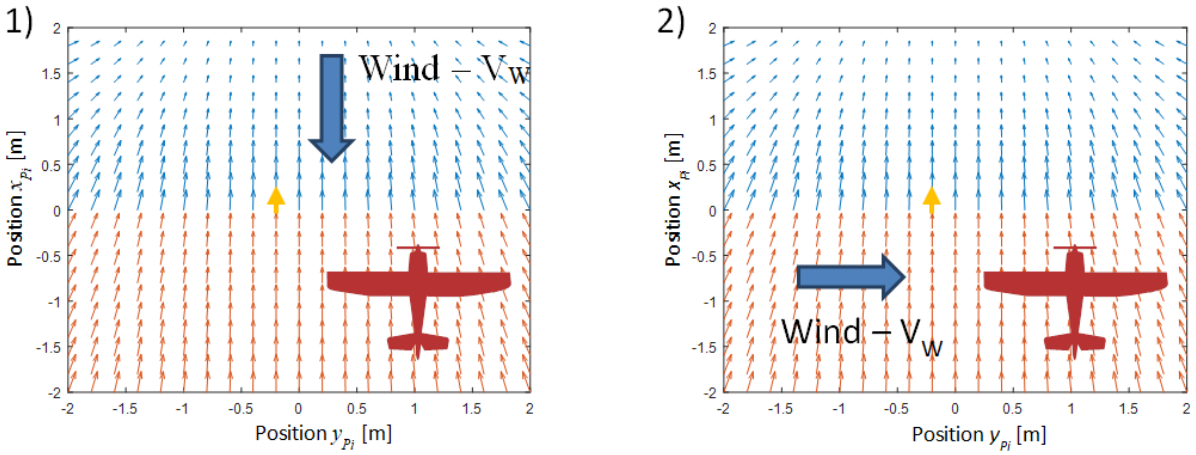

Fig. 6. Simulated scenarios of a step change of wind velocity to verify lateral and longitudinal controls of UAV. UAV - unmanned aerial vehicle

5. RESULTS

In each simulation, positions of the virtual tracked point and the starting point of the UAV overlap, and paths of the virtual point are designed as straight lines. Since the UAV tracks the virtual point and the initial airspeeds of both are zero, there should be inertia between the movements of the UAV and the tracked virtual point. In the first considered case, the direction of the simulated step change of wind velocity is exactly opposite to the direction of the virtual point's movement. Therefore, it should increase tracking error on the x_{Pi} axis as steady-state tracking error, i.e. wind drift. In the second case, the direction of the wind is perpendicular to the line of the virtual point's path. Thus, the tracking error should increase on the y_{Pi} axis.

Firstly, it should be examined how the previous approach of AAPF is able to decrease tracking error in the steady state. To verify this, numerical simulations were prepared according to the second scenario for different values of coefficients α (0.1, 0.9), β (0.1, 0.9) and γ (0.1, 0.9) (Eq. 3), and δ_{x1}, δ_{x2}, δ_y and δ_z equal zero. Time plots of tracking errors on each axis are presented in Fig. 7. The amplitude of the step change of wind velocity at $t = 100$ s is 1 m/s.

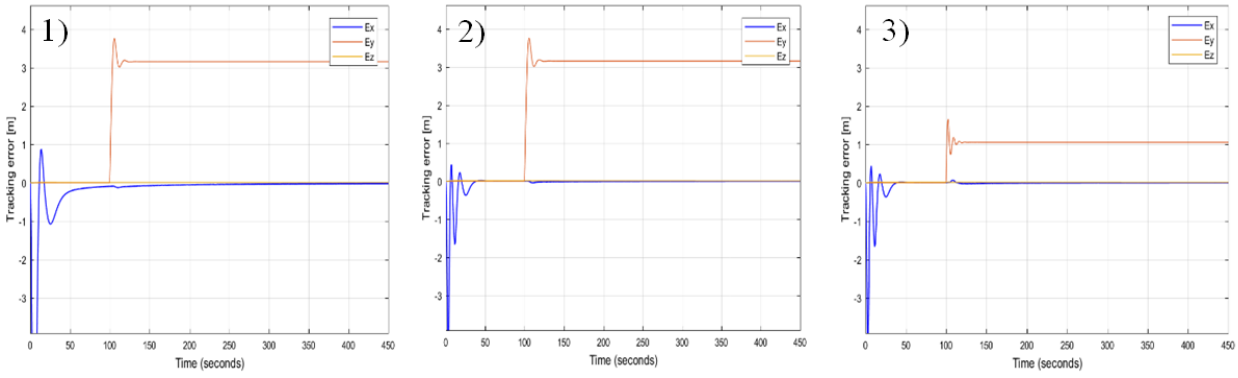

Fig. 7. Time plots of tracking errors on axes x_{Pi}, y_{Pi} and z_{Pi} for the following values of coefficients α, β and γ: (1) $\alpha = 0.1$, $\beta = 0.1$ and $\gamma = 0.1$, (2) $\alpha = 0.9$, $\beta = 0.9$ and $\gamma = 0.1$, (3) $\alpha = 0.9$, $\beta = 0.9$ and $\gamma = 0.9$

According to the first scenario (Fig. 6), different values of δ_{x1}, δ_{x2} were used to observe minimisation of the tracking error on the x_{Pi} axis as the result of a step change of wind velocity at $t = 200$ s. on this axis with an amplitude equal to 1 m/s. Simulation results are given in Fig. 8.

In Fig. 6, it can be seen that time plots of E_x are independent from the values of δ_{x1} (Fig. 8.1–8.4). This is because this coefficient regulates the gain of integral I_X for $x_{Pi} > 0$, when the UAV is flying behind the virtual point, and thus $x_{Pi} < 0$ and $I_X < 0$. This is in accordance with the assumptions of guidance rules defined by Eqs (3), (4), (6), (7) and (8). On the other hand, in Figs. 8.5–8.8, a decrement of tracking error E_x can be observed for higher values of δ_{x2}. A side effect of the action of integral I_X is transient and quickly fading oscillations whose frequency grows with the value of δ_{x2}. Amplitudes of these oscillations are less than 1 m, and their durations are less than 25 s. Therefore, they should not have a significant impact on the effectiveness of flight guidance based on the proposed approach.

In the second scenario, where the wind direction is perpendicular to the simulated flight path of the virtual point, only coefficient δ_y matters, because it is related to integral I_Y. The rest of the parameters are as follows: α, β and γ remain the same, $\delta_{x1} = 1$ and $\delta_{x2} = 1$. In Figs. 9.1–9.4, time plots of tracking errors are presented for a value of δ_y equal to, respectively, 0, 0.1, 1 and 5.

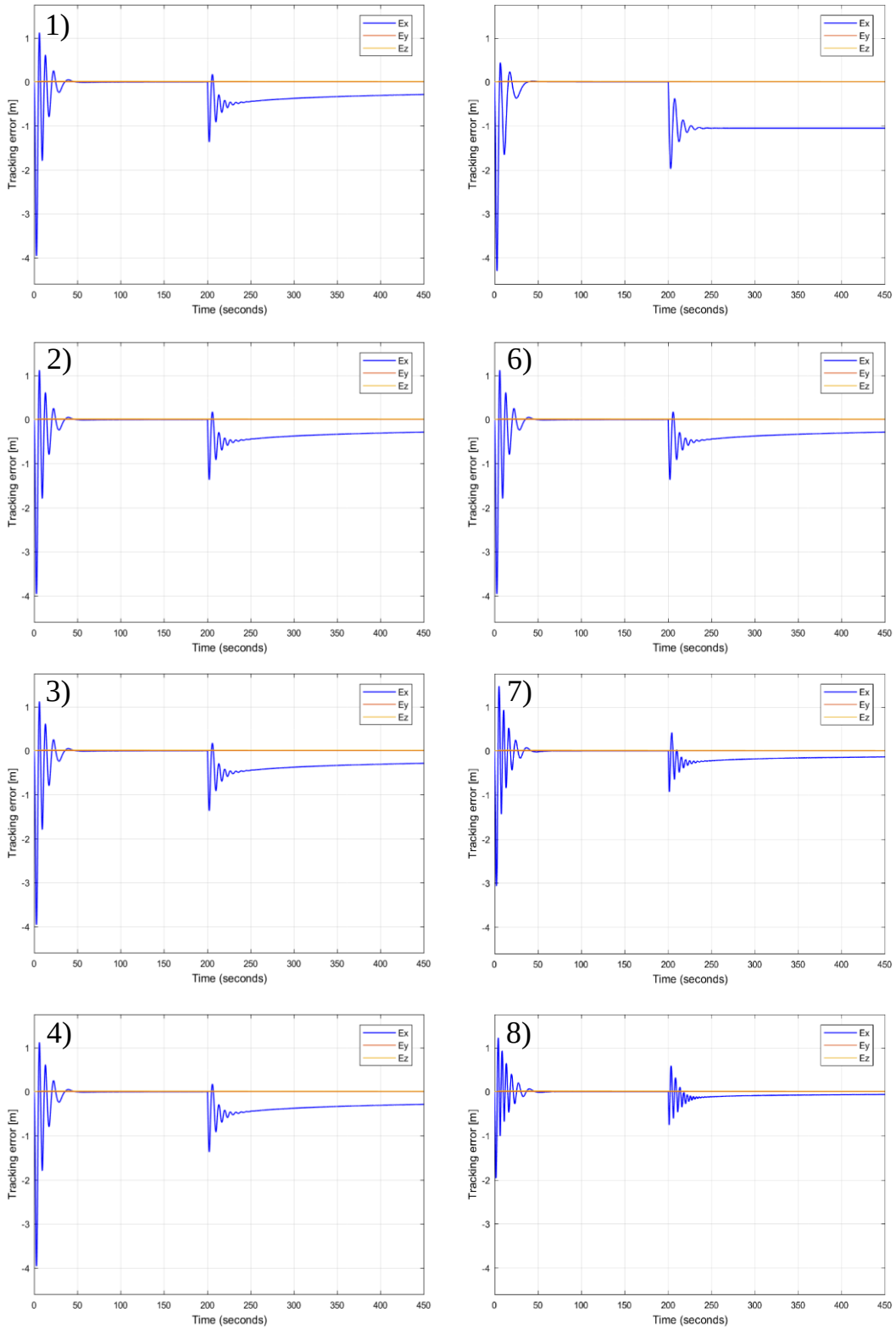

Fig. 8. Time plots of tracking errors on axes x_{Pi}, y_{Pi} and z_{Pi} for the following values of coefficients δ_{x1}, δ_{x2}, δ_y and δ_z: (1) $\delta_{x1} = 0$, $\delta_{x2} = 0.1$, $\delta_y = 0$ and $\delta_z = 0$, (2) $\delta_{x1} = 0.5$, $\delta_{x2} = 0.1$, $\delta_y = 0$ and $\delta_z = 0$, (3) $\delta_{x1} = 1$, $\delta_{x2} = 0.1$, $\delta_y = 0$ and $\delta_z = 0$, (4) $\delta_{x1} = 1.5$, $\delta_{x2} = 0.1$, $\delta_y = 0$ and $\delta_z = 0$, (5) $\delta_{x1} = 1$, $\delta_{x2} = 0$, $\delta_y = 0$ and $\delta_z = 0$, (6) $\delta_{x1} = 1$, $\delta_{x2} = 0.1$, $\delta_y = 0$ and $\delta_z = 0$, (7) $\delta_{x1} = 1$, $\delta_{x2} = 1$, $\delta_y = 0$ and $\delta_z = 0$, (8) $\delta_{x1} = 1$, $\delta_{x2} = 10$, $\delta_y = 0$ and $\delta_z = 0$

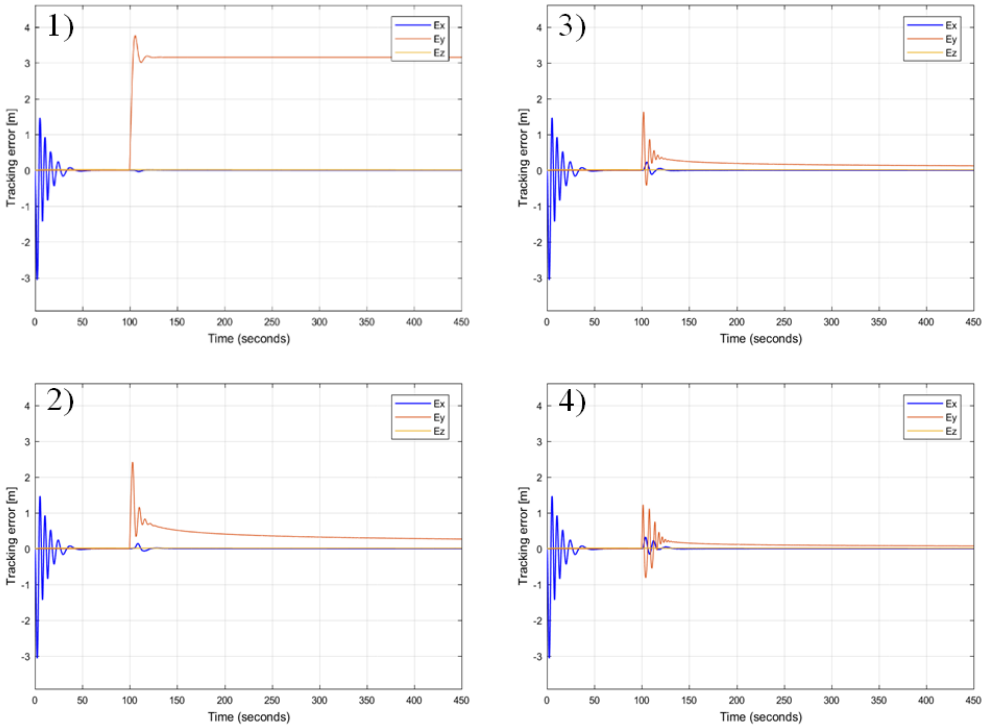

Fig. 9. Time plots of tracking errors on axes x_{Pi}, y_{Pi} and z_{Pi} for the following values of coefficients δ_{x1}, δ_{x2}, δy and δ_z: $\delta_{x1} = 1$, $\delta_{x2} = 1$, (1) $\delta_y = 0$, (2) $\delta_y = 0.1$, (3) $\delta_y = 1$, (4) $\delta_y = 5$

Based on Fig. 7, it is possible to conclude that α and β improve guidance dynamics on the x_{Pi} axis by increasing the slope of potential function U_i^S on both sides of the $y_{Pi} - z_{Pi}$ plane. Oscillations of tracking error on axis x_{Pi} are caused by inertia in position tracking at instant $t = 0$ and UAV guidance switching between acceleration and deceleration zones separated by the $y_{Pi} - z_{Pi}$ plane. The frequency of this oscillation increases with the increment of the potential function's slope caused by higher values of α and β. As would be expected, values of α and β have no effect on tracking error E_y on the y_{Pi} axis. This tracking error can be decreased by increasing the value of γ, which can be observed by comparing Figs 7 (2 and 3). However, E_y still does not decrease over time; thus, it should be considered as steady-state tracking error caused by wind drift.

Next, non-zero values of δ_{x1}, δ_{x2}, δ_y, and δ_z are applied in the novel definitions of gradient ∇U_i^{AD} and velocity vector field V_i^{AD} to include integrals I_x, I_Y, and I_Z. Values of α, β and γ are constant and are, respectively, 0.9, 0.9 and 0.1.

Also, in this case, a value of δ_y higher than 0 guarantees that tracking error E_y decreases over time. The magnitude of decrement increases with the value of δ_y, but simultaneously, the amplitude and frequency of oscillations of tracking error E_y also grow. However, these oscillations are still transient and fast-fading, and they have no bearing on the effectiveness of the approach to minimisation of tracking error in the steady state.

6. CONCLUSION

Both methods based on AAPFs have significance to the problem of position tracking by nonholonomic vehicles such as fixed-wing UAVs. They improve the stability and the precision of position tracking during manoeuvres. However, they do not prevent against position tracking errors in the steady state, caused by wind drift in windy environments. Therefore, definitions of the gradient of the asymmetrical potential function and the VVF should be dependent on integrals of tracking errors, as in the definition of a proportional–integral–derivative controller, where the integral is used to minimise steady-state errors. As presented, numerical simulation results confirm that such modification will allow for reduction of tracking errors asymptotically in the steady state. This is because of the fact that integrals of tracking errors are variable gain coefficients which modify the gradient according to the growth of the steady-state error, in a manner identical to the increment of the potential function's slope. This effect is presented in Figs 8 and 9, where time plots of tracking errors for different values of integrals' coefficients, δ_{x1}, δ_{x2}, and δ_y, compare the effectiveness of tracking error minimisation. Increasing values of these integrals' coefficients amplify the magnitude of decrement but simultaneously increase the frequency of oscillation. Fortunately, oscillations are quickly suppressed by inertia in the unmanned aerial vehicle's dynamics. Therefore, integrals' coefficients, δ_{x1}, δ_{x2}, δ_y, and δ_z, as well as coefficients of the potential function, α, β and γ, should be precisely adjusted to the dynamics specific to each considered fixed-wing UAVs' construction.

In summary, the novel self-adaptive approach to the asymmetrical potential function makes the position tracking problem more resistant to external disturbances in windy environments, which is crucial for fixed-wing UAVs. This is not possible through the usage of other methods of path planning, which are based on symmetrical APFs.

REFERENCES

1. **Ambroziak L., Gosiewski Z.** (2015), Two Stage Switching Control for Autonomous Formation Flight of Unmanned Aerial Vehicles, *Aerospace Science and Technology*, Vol. 46, 2015, pp. 221-226,

2. **Ambroziak L., Kondratiuk M., Ciezkowski M., Kownacki C.** (2018), Hardware in the Loop Tests of the Potential Field-Based Algorithm for Formation Flight Control of Unmanned Aerial Vehicles, Mechatronic Systems and Materials 2018, Zakopane, *AIP Conference Proceedings* 2029, 020002-1–020002-10.
3. **Barnes L., Fields M. and Valavanis K.** (2007), Unmanned Ground Vehicle Swarm Formation Control Using Potential Fields, in *Mediterranean Conference on Control and Automation*, Athens.
4. **Bennet D. J., McInnes C. R.** (2008) Space Craft Formation Flying Using Bifurcating Potential Fields, in *International Astronautical Congress*.
5. **Bennet D. J., McInnes C. R.** (2011), Autonomous Three-Dimensional Formation Flight for a Swarm of Unmanned Aerial Vehicles, *Journal of Gudiance, Control, and Dynamics*, vol. 34, no. 6, pp. 1899-1908.
6. **Budiyanto A., Cahyadi A., Adji T. B., Wahyunggoro O.** (2015), UAV Obstacle Avoidance Using Potential Field Under Dynamic Environment, in *2015 International Conference on Control, Electronics, Renewable Energy and Communications*, Bandung.
7. **Cetin O., Yilmaz G.** (2016), Real-time Autonomous UAV Formation Flight with Collision and Obstacle Avoidance in Unknown Environment, *Journal of Intelligent & Robotic Systems*, vol. 84, no. 1, pp. 415-433.
8. **Chen Y., Luo G., Mei Y., Yu J. and Su X.** (2016), UAV Path Planning Using Artificial Potential Field Method Updated by Optimal Control Theory, *International Journal of System Science*, vol. 47, no. 6, pp. 1407-1420.
9. **Chen Y., Yu J., Su X., Luo G.** (2015), Path Planning for Multi-UAV Formation, *Journal of Intelligent & Robotic Systems*, vol. 77, no. 1, pp. 229-246.
10. **Frew E. W., Lawrence D. A., Dixon C., Elston J., Pisano W. J.** (2007), Lyapunov Guidance Vector Fields for Unmnned Aircraft Applications, in *IEEE American Control Conference*.
11. **Gosiewski Z., Ambroziak L.** (2012), Formation Flight Control Scheme for Unmanned Aerial Vehicles, *Lecture Notes in Control and Information Science*, vol. 422, pp. 331-340, 2012,
12. **Hatton R.L., Choset H.** (2011). Geometric Motion Planning: the Local Connection, Stokes' Theorem, and the Importance of Coordinate Choice. *The International Journal of Robotics Research*, 30(8), pp.988-1014,
13. **Khuswendi T., Hindersah H., Adiprawita W.** (2011), UAV Path Planning Using Potential Field and Modified Receding Horizon A* 3D Algorithm, in *Proceedings of the 2011 International Conference on Electrical Engineering and Informatics*.
14. **Kokume N., Uchiyama K.** (2010), Guidance Law Based on Bifurcating Velocity Field for Formation Flight, in *AIAA Guidance, Navigation, and Control Conference*.
15. **Kowalczyk W., Kozłowski K.** (2004), Artificial Potential Based Control for a Large-Scale Formation of Mobile Robots., in *Proceedings of the Fourth International Workshop on Robot Motion and Control*.
16. **Kownacki C.** (2016), Multi-UAV Flight Using Virtual Structure Combined with Behavioral Approach, *Acta Mechanica et Automatica*, Vol. 10, No 2. 92-99.
17. **Kownacki C., Ambroziak L.** (2017), Local and Asymmetrical Potential Field Approach to Leader Tracking Problem in Rigid Formations of Fixed-Wing UAVs, *Aerospace Science and Technology*, Vol. 68, September 2017, pp. 465-474.
18. **Kownacki C., Ambroziak L.** (2019), Adaptation Mechanism of Asymmetrical Potential Field Improving Precision of Position Tracking in the Case of Non-Holonomic UAVs, *Robotica*, doi: https://doi.org/10.1017/S0263574719000286, published online: 10 April 2019, pp. 1-12,
19. **Kownacki C., Ołdziej O.** (2016), Fixed-wing UAVs Flock Control through Cohesion and Repulsion Behaviours Combined with a Leadership, *International Journal of Advanced Robotic Systems*, vol. 13, p. DOI: 10.5772/62249.
20. **Li K., Han X., Qi G.** (2009), Formation and Obstacle-Avoidance control for Mobile Swarm Robots Based on Artificial Potential Field, in *Conference on Robotics and Biomimetics*.
21. **Mukherjee R., Anderson D.P.** (1993), Nonholonomic Motion Planning Using Stokes' Theorem. In: *IEEE International Conference on Robotics and Automation*, pp. 802–809.
22. **Nagao Y., Uchiyama K.** (2014), Formation Flight of Fixed-Wing UAVs Using Artificial Potential Field, in *29th Congress of the International Council of the Aerospace Sciences*, St. Petersburg.
23. **Nelson D. R., Barber D. B., McLain T. W., Beard R. W.** (2007), Vector Field Path Following for Miniature Air Vehicles, *IEEE Transactions on Robotics*, vol. 23, no. 3, pp. 519-529.
24. **Nieuwenhuisen M., Schadler M., Behnke S.** (2013), Predictive Potential Field-Based Collision Avoidance for Multicopters, International Archives of Photogrammetry, *Remote Sensing and Spatial Information Sciences*, Vols. XL-1/W2.
25. **Suzuki M., Uchiyama K.** (2010), Autonomous Formation Flight Using Bifurcating Potential Fields, in *27th International Congress of the Aeronautical Sciences*, Nice.
26. **Suzuki M., Uchiyama K.** (2011), Three-Dimensional Formation Flying Using Bifurcating Potential Fields, in AIAA Guidance, *Navigation, and Control Conference*, Chicago.
27. **Tobias P., Krogstad T. R., Gravdahl J. T.** (2008), UAV Formation Flight Using 3D Potential Field, in *16th Mediterranean Conference on Control and Automation*.
28. **Virágh C., Vásárhelyi G., Tarcai N., Szörényi T., Somorjai G., Nepusz T., Vicsek T.** (2014), Flocking Algorithm for Autonomous Flying Robots, *Bioinspiration & Biomimetics*, vol. 9, no. 2, p. 025012.

Acknowledgments: The research was funded by statutory funds of Department of Robotics and Mechatronics, Faculty of Mechanical Engineering, Białystok University of Technology (WZ/1/WM/2019).